Suzaku Observations of the Dwarf Nova V893 Scorpii: the Discovery of a Partial X-ray Eclipse

K. Mukai

CRESST and X-ray Astrophysics Laboratory, NASA/GSFC, Greenbelt, MD 20771; and Department of Physics, University of Maryland, Baltimore County, 1000 Hilltop Circle, Baltimore, MD 21250.

Koji.Mukai@nasa.gov

E. Zietsman

Department of Astronomy, University of Cape Town, Private Bag X3, Rondebosch 7701, South Africa.

and

M. Still

Mullard Space Science Laboratory, University College London, Holmbury St. Mary, Dorking, Surrey RH5 6NT, UK.

mds@mssl.ucl.ac.uk

ABSTRACT

V893 Sco is an eclipsing dwarf nova that had attracted little attention from X-ray astronomers until it was proposed as the identification of an *RXTE* all-sky slew survey (XSS) source. Here we report on the pointed X-ray observations of this object using *Suzaku*. We confirm V893 Sco to be X-ray bright, whose spectrum is highly absorbed for a dwarf nova. We have also discovered a partial X-ray eclipse in V893 Sco. This is the first time that a partial eclipse is seen in X-ray light curves of a dwarf nova. We have successfully modeled the gross features of the optical and X-ray eclipse light curves using a boundary layer geometry of the X-ray emission region. Future observations may lead to confirmation of this basic picture, and allow us to place tight constraints on the size of the X-ray emission region. The partial X-ray eclipse therefore should make V893 Sco a key object in understanding the physics of accretion in quiescent dwarf nova.

Subject headings: Stars: novae, cataclysmic variables — stars: individual (V893 Sco) — X-rays: binaries

1. Introduction

Cataclysmic variables (CVs), in which the white dwarf primary accretes from a Roche-lobe filling, late-type secondary (see Warner 1995 for a comprehensive review), are an excellent laboratory for the physics of accretion. In a subset of CVs, the primary possesses a strong enough magnetic field to channel the accretion onto magnetic pole region(s). However, the majority of CVs are non-magnetic and accretion proceeds via a disk. If the mass input rate is low, as is the case for systems below the period gap (i.e., orbital period shorter than ∼2 hrs), the disk remains faint most of the time (quiescence), occasionally brightening to produce outbursts. Such systems are called dwarf novae. Dwarf nova outbursts are explained in the framework of the disk instability model; while the framework is successful, there are details that defy the prediction of the basic version of the disk instability model (Lasota 2001). For example, the observed X-ray luminosity of quiescent dwarf novae is higher than the basic disk instability model predicts, in which the material is expected to pile up in the disk to be emptied onto the white dwarf only during outburst. The observed X-rays, in contrast, show that the white dwarf is actively accreting even during quiescence. Since the quiescent disks in dwarf novae are too cold to emit X-rays, the specific origin of the X-rays must be the volume immediately next to the white dwarf surface, such as an optically thin boundary layer (Ptterson & Raymond 1985). Proposed modifications of the theory includes the coronal siphon flow (Meyer & Meyer-Hofmeister 1994), which might lead to accretion over a much wider area of the white dwarf surface than through a boundary layer, and a weakly magnetic white dwarf (Livio & Pringle 1992). In the latter model, the magnetic field is too weak to control the accretion flow during outburst, but strong enough to do so during quiescence, so that quiescent dwarf novae resemble intermediate polars (IPs).

IPs (also called DQ Her type systems) are a subset of magnetic CVs (see Patterson 1994 for a review), in which the primary's magnetic field disrupts the inner accretion disk, channeling the flow to the magnetic polar region(s). Their defining characteristic is the coherent photometric modulation at the spin period of the white dwarf, which is significantly less than the orbital period. Although several IPs also show outbursts, they tend to be rarer and shorter in duration than the dwarf nova outbursts (see Mhlahlo et al. 2007 and references therein).

V893 Sco is an eclipsing (Bruch et al. 2000) dwarf nova with an orbital period of 1.8 hr (Thorstensen 1999). According to Kato et al. (2002), V893 Sco has a quiescent magnitude of ∼14.5, and has an outburst every ∼30 days during which it reaches magnitude ∼12.5. Extensive photometry by Warner and collaborators (Warner et al. 2003; Pretorius et al. 2006) have revealed quasi-periodic oscillations and dwarf nova oscillations in V893 Sco, but a strictly periodic signal was never found. Therefore, existing optical data point strongly

towards a dwarf nova classification and argue against an IP classification. Thus, V893 Sco joins a growing number of eclipsing dwarf novae below the period gap, summarized in Table 1, which is taken from "update RKcat 7.9[1]" of the Ritter & Kolb catalog (Ritter & Kolb 2003). We have arranged the objects in order of quiescent brightness; since RKcat 7.9 lists V893 Sco at 15.5, that is what we used here. Had we adopted the Kato et al. (2002) magnitude of 14.5 instead, V893 Sco would have been the first object in this table.

The visible light output of a quiescent dwarf nova is often dominated by the bright spot, where the accretion stream hits the disk, and by the photospheric emission of the white dwarf. When such a system is deeply eclipsed, two distinct sets of rapid transitions (ingress and egress) are observed in the optical light curves, since the bright spot eclipse is offset to a somewhat later phase. Systems for which two components are seen to be eclipsed are indicated in Table 1, and provide an invaluable opportunity to constrain the system parameters tightly.

No evidence for such a double eclipse has been seen in V893 Sco. Citing the variable shape of the eclipses and the relatively small eclipse amplitude (often less than 0.75 mag), Bruch et al. (2000) argue for a grazing eclipse of the hot spot and the disk, but not of the white dwarf. On the other hand, Matsumoto et al. (2000) argue that the white dwarf is eclipsed, based on the fact that the spectroscopic conjunction of the disk (the red-to-blue crossing of the emission line radial velocities) occurs at mid-eclipse. From the radial velocity curves, they also infer a white dwarf mass of $\sim$0.5–0.6 $M_\odot$ and a mass ratio of $\sim$0.2–0.3. However, Mason et al. (2001) prefer a higher mass (0.89 $M_\odot$) white dwarf and an inclination angle of 72.5 degrees based on their analysis of the emission line radial velocities, although this value depends in part on the assumed mass-radius relationship for the secondary.

Despite the lack of double eclipses and a consensus on the system parameters, the eclipsing nature of V893 Sco makes it an important target for detailed studies. Moreover, it is a nearby system with parallax-estimated distance of 155^{+58}_{-34} pc (Thorstensen 2003).

Although the *ROSAT* detection was already noted by Kato et al. (1998), V893 Sco did not draw the attention of X-ray astronomers until it was listed among the *RXTE* all-sky slew survey (XSS) sources (Revnivtsev et al. 2004), along with three other dwarf novae (SS Aur, V426 Oph, and SU UMa). The estimated luminosities of these 4 systems are all just under 10^{32} ergs s^{-1} in the 2–10 keV band, placing them near the upper end for non-magnetic CVs (10^{30}–3×10^{32} in 0.1–100 keV for the *ASCA* sample; Baskill et al. 2005). The XSS is based on the data taken during slews of the non-imaging *RXTE* PCA detector. For relatively faint sources such as these dwarf novae, the positional errors are considerable, and

[1]http://physics.open.ac.uk/RKcat/

misidentification is a possibility. Hence it is important to confirm the proposed identification of XSS dwarf novae. This is particularly true for V893 Sco, which had never been the subject of a pointed X-ray observation above 2 keV. Although V893 Sco is securely detected as a RASS source, the ratio of XSS (2.38 c/s in the 3–8 keV band) to RASS (0.35) count rates is high, compared to, e.g., SS Aur which has the same RASS count rate but was detected at 0.75 c/s in the XSS 3–8 keV band. This leaves open the possibility that V893 Sco is only a partial contributor to the XSS flux. For this reason and also because of the potential return in studying the X-ray properties of this eclipsing dwarf nova, we performed a pointed observation using *Suzaku*, along with contemporaneous optical photometry.

2. Observations and Data Reduction

We observed V893 Sco with *Suzaku* (Mitsuda et al. 2007) between 2006 Aug 26 09:40 and Aug 27 01:20 UT (sequence number 401041010). There are two types of co-aligned instruments on-board *Suzaku*, which are: 4 units of the CCD-based X-ray imaging spectrometer (XIS), each behin its X-ray telescope (XRT), and the non-imaging hard X-ray detector (HXD). As the source is relatively faint for a non-imaging instrument and the exposure time short, we did not analyze the HXD data, a decision that we justify at the end of §3.1.

We started from data processed using the V2.0.6.13 pipeline. We then updated the energy scale calibration using the 2008 Feb 1 release of the calibration database. Initially we applied the standard screening criteria: attitude control system in nominal mode, pointing within 1.5 arcmin of the mean direction, XIS data rate medium or high, the satellite outside the South Atlantic Anomaly (SAA), at least 436 s after the last SAA passage, elevation above Earth limb $> 5^\circ$, elevation about the bright Earth limb $> 20^\circ$. We then experimented with relaxing some of the standard criteria to maximize the phase coverage of the observation. We found that relaxing the post-SAA passage limit from 436 s to 180 s, and the bright Earth limb limit from 20° to 15° did not noticeably increase the noise level of our data. With this modification, the total XIS exposure time was 19,174 s, representing a 670 s increase compared to the standard screening.

We used a 3 arcmin radius extraction region for the source and 7.5 and 4 arcmin radius annular extraction region for the background, both centered on the measured location of V893 Sco. For spectroscopy, we summed the data and the responses of the three XIS units with frontside illuminated (FI) CCD chips, because they have nearly identical responses. We fitted the data from XIS1 (with the backside illuminated, or BI, CCD chip) simultaneously with the sum of FI spectra. For photometry, we added background subtracted light curves

from all 4 XIS units over the 0.4 keV (FI)/0.3 keV (BI) to 10 keV bandpass using 8 s bins, preserving the original time resolution of the XIS data. We also extracted light curves below 2 keV, in the 2–4 keV band, and above 4 keV to investigate possible energy dependence.

We also carried out optical photometry of V893 Sco on the nights of 25, 26, and 27 August 2006 using the University of Cape Town CCD Photometer (UCTCCD; O'Donoghue 1995) on the South African Astronomical Observatory (SAAO) 1.9m telescope. The detector is a Wright Instruments Peltier-cooled CCD with a thinned and back-illuminated EEV P86321/T chip. It was used in frame-transfer mode where one half of the CCD is masked and used as a readout area, allowing exposures to be made with essentially no "dead" time between exposures. On the 1.9m telescope, the pixels on the detector correspond to 0.13 arcsec so that it is normal to use 3x3 or greater pre-binning, unless the seeing is better than about 1 arcsec, to ensure optimal data-extraction. Because V893 Sco is relatively bright, integration times of 6 seconds were used on all nights. All observations were made in white light. The CCD was pre-binned at 5x5, 4x4, and 3x3 for the three nights respectively.

Observations were reduced at the telescope using a custom pipeline, which allows the observer to select suitable comparison stars and judge observations. The conventional procedure of reducing observations were followed (bias subtraction, flatfield correction etc.) after which the stellar brightnesses were extracted using the method described in Schechter et al. (1993). Differential corrections were made by using the lightcurve of the brightest nearby star. Due to the small size of the UCTCCD (50x34 arcsec^2 on the 1.9m telescope) the only available comparison stars were somewhat fainter than V893 Sco but they were nevertheless used as the differentially corrected lightcurves were deemed to be of better quality than the uncorrected ones.

3. Results

3.1. X-ray Spectrum

The X-ray spectrum of V893 Sco is typical of dwarf novae in that it consists of an absorbed bremsstrahlung-like continuum and a prominent He-like Fe Kα at 6.7 keV (Baskill et al. 2005; Pandel et al. 2005). The latter indicates the origin in an optically-thin, thermal plasma. We therefore use the `mkcflow` model that was originally developed for the cooling flow in clusters of galaxies, but was successfully applied to X-ray emission from CVs (Mukai et al. 2003). In its original context, the cooling flow model assumes a steady-state with a large reservoir of plasma in the outer parts of the cluster at the maximum temperature, kT$_{max}$; the plasma cools by emitting X-rays with no additional energy input. In the CV

context, fresh accreting plasma is shock-heated to kT_{max} every second, which must cool before it can settle onto the white dwarf surface. Therefore the steady-state assumption is also appropriate in the CV case, and the model describes the physics correctly in the limit in which X-ray emission provides the only cooling mechanism and no additional heating occurs once the plasma is shocked (cf. the tall shock solution appropriate for some CVs; Cropper et al. 1999).

We also use the single temperature plasma model `mekal` for comparison, for convenience and for ease of comparison, since this model is often used to fit the CV spectra. However, we note that it is an unphysical model for CVs, since post-shock plasma in CVs loses energy by emitting X-rays and therefore must cool, and in doing so the density increases, making it a more efficient emitter of X-rays. The X-ray emisison in CVs is therefore multi-temperature by nature.

We present the results of our fit in Figure 1 (for the `mkcflow` model) and in Table 2 (for both models). In both cases, the use of a single absorber (using the `wabs` model) resulted in significant residuals particularly below 1 keV (see the middle panel of Figure 1). The fitted N_H of $> 5 \times 10^{21}$ cm^{-2} is too high to be the interstellar column towards V893 Sco at d=155 pc; even the total Galactic column in this direction is only 1.4×10^{21} cm^{-2} (Dickey & Lockman 1990) as reported by the HEASARC Nh tool[2]. Thus, we conclude that an intrinsic absorber must be present in the V893 Sco binary system. For example, our line of sight to the boundary layer may pass through the inner accretion disk (van Teeseling et al. 1996).

The low energy residual was successfully removed by adding an additional partial covering absorber (`pcfabs`) (see the top and the bottom panels of Figure 1 and Table 2). We also tried using an additional emission component instead, while keeping just a single `wabs` absorber. These were not as successful at removing the residuals as the complex absorber: adding a low temperature `mekal` to `mkcflow` resulted in χ^2_ν=0.813 with residuals below 0.7 keV, and the addition of a blackbody resulted in χ^2_ν=0.793 with residuals below 0.6 keV, compared to χ^2_ν=0.766 for the complex absorber fit. Thus, we prefer the partial covering absorber interpretation, also because this is a natural consequence if the X-ray emission region and the absorber are comparable in size.

This intrinsic absorber also offers a partial explanation for the high XSS to RASS count ratio: since the source is heavily absorbed, the RASS count rate is suppressed while the XSS count rates are not. However, a detailed comparison shows that this is not the complete story. Using the best-fit partial-covering `mkcflow` model, the *Suzaku* spectrum corresponds to a *ROSAT* PSPC (on-axis) count rate of 0.24 ct s^{-1}, compared to the vignetting-corrected

[2]http://heasarc.gsfc.nasa.gov/cgi-bin/Tools/w3nh/w3nh.pl

value of 0.35 ct s^{-1} in the RASS, or an observed-to-predicted ratio of ∼1.5. For the *RXTE* PCA, predictions (XSS measurements) are 1.35 ct s^{-1} (2.38) in the 3–8 keV band for a ratio of ∼1.8 and 0.51 ct s^{-1} (0.96) for ∼1.9 in the 8–20 keV band. That is, the differences between the predictions from *Suzaku* and the observed values are higher for higher energies. In addition to source variability, which is expected in a dwarf nova, the possibility of an additional source within the PCA field of view should therefore be kept in mind.

A prominent emission line at 6.7 keV from the He-like ion of Fe was already obvious in the broad-band view (Figure 1). To investigate this further, we fitted an absorbed bremsstrahlung continuum and three Gaussians in the 5–10 keV range (Figure 2 and Table 3). In addition to the dominant 6.7 keV line, we also detected both the H-like line (6.97 keV) and the fluorescent line at 6.4 keV. While the H-like and He-like lines originate in the hot plasma and are included in thin thermal plasma code (`mekal` and `mkcflow`), the 6.4 keV line is not. This line is almost certainly due to reflection on the white dwarf surface (Done & Osborne 1999). Although we did not include the fluorescent line in the global fit, it is sufficiently weak not to have affected the quality of the fit or the derived parameter values.

The 2–10 keV absorbed flux of V893 Sco is 1.7×10^{-11} ergs cm^{-2}s^{-1}, corresponding to 4.9×10^{31} ergs s^{-1} at 155 pc. The 0.4–2 keV absorbed flux is 3.0×10^{-12} ergs cm^{-2}s^{-1}, while the extrapolated flux of V893 Sco above 10 keV is $< 1 \times 10^{-11}$ ergs cm^{-2}s^{-1}. This justifies our choice not to analyze the HXD data, since a source at this flux level is undetectable given the current systematic uncertainties in the background reconstruction. The estimated bolometric X-ray luminosity depends on the choice of spectral models (see Table 2), but may be as high as 1.4×10^{32} ergs s^{-1}, placing V893 Sco among the most X-ray luminous dwarf nova (Baskill et al. 2005).

3.2. Optical Light Curves

We had three purposes in mind for obtaining optical photometry of V893 Sco contemporaneously with the *Suzaku* observations. First, we wished to ascertain the outburst status of the object. The instrumental white light magnitudes, as measured with the SAAO 1.9 m telescope, were in the range 11.0–11.5, 11.5–12.0, and 11.2–11.8 outside the eclipse, respectively, on the nights of Aug 25, 26, and 27. Since there is a known offset of approximately 3.0–3.2 magnitudes with respect to the standard V band for the typical spectrum of a CV, V893 Sco had V magnitudes of 14.0–15.0 out of eclipse on these nights. That is, V893 Sco was in quiescence during the *Suzaku* observations.

Our second purpose was to check the orbital ephemeris. We therefore folded the SAAO

light curves on the ephemeris of Bruch et al. (2000) and found that the eclipse occurred ∼0.17 cycles earlier than predicted. We therefore measured the individual times of eclipses as follows. We measured by hand the end of the steep part of the egress, approximately 0.015 cycle after the mid-eclipse, where the light curve slope changed significantly. We also noted the times of the slight change in slope during ingress, ∼0.015 cycle before the mid-eclipse, even though there often was ambiguity exactly where this happened. The results for the 6 eclipses (2 were observed on each of the three nights) are listed in Table 4, along with the brightness level relative to the faintest point during that eclipse. On average, we measured a slight steepening of the gradient at Bruch et al. phase 0.8093±0.005, ∼0.56 mag above mid eclipse; and the end of the steep part of the egress at Bruch et al. phase 0.8385±0.0011, ∼0.47 mag above. We therefore applied a offset of −0.176 to the phases calculated using the Bruch et al. (2000) ephemeris. This is equivalent to adopting a linear ephemeris with a period of 0.075961467 d (cf. 0.07596185±0.00000012 d of the ephemeris) while keeping the same epoch for cycle 0, although the time gap of 7 years between the Bruch et al. observation and ours is long enough that a quadratic ephemeris may be more realistic.

The final purpose of the optical photometry was a detailed comparison of the X-ray and optical light curves. We will present our analysis of the X-ray light curves in §3.3, and report on our modeling of both the optical and X-ray light curves in §4.3.

3.3. X-ray Light Curves

We present the *Suzaku* light curve of V893 Sco against time and relative cycle counts (since cycle 34890.0 of Bruch et al. ephemeris, adjusted as described in §3.2) in Figure 3. Due to the restrictions of low Earth orbit satellites, the *Suzaku* coverage has many gaps, with unfortunately little strict overlap with the SAAO photometry. The phase coverage is highly uneven: it can be seen that phase interval 0.6–0.9, for example, is poorly covered. The *Suzaku* count rate is variable at all orbital phases, but there are dips whenever the phase of the optical eclipse is covered. The *Suzaku* data cover the eclipse phase completely twice (at relative cycle count 3.0 and 4.0); in addition, they cover a part of the ingress once (5.0, as the satellite was approaching the night-side limb of the Earth), and the egress once (8.0, as the satellite emerged from the daylight limb of the Earth).

In the folded representation (Figure 4), the X-ray light curve shows a clear partial eclipse, coincident with the optical eclipse. The out-of-eclipse light curve is also clearly variable. However, given the poor phase coverage of the *Suzaku* data, it is premature to consider any orbital modulations outside the eclipse. The apparently greater amplitude of variability during the second half of the orbital cycle (0.5–1.0), in particular, is probably due to the

poorer coverage of these phases. We Fourier-transformed the light curves, with or without the eclipses, for the total XIS band as well as in three energy bands. On the one hand, the results are consistent with a presence of a strong red noise but no coherent, non-orbital periodicities. On the other hand, our sensitivity to periods longer than ∼2,000 s is severely compromised by the data gaps.

We also investigated the potential energy dependence of the eclipse. In the left half of Figure 5, we show the eclipse profiles in three energy bands, as histograms. Solid lines, repeated in all three panels, are the eclipse profile for the total band. The lack of strong energy dependence in the profile proves that this is not an absorption event, such as an X-ray dip due to the outer rim of the disk, or occultaion by an extended atmosphere of the secondary.

We also investigate how repeatable this phenomenon was. A comparison between the average profile (shown in Figure 4) and individual cycles would be dominated by the slow (>1,000 s) variations in the source brightness. Therefore, we first scaled each eclipse by the average out-of-eclipse count rates immediately before (phase 0.90–0.94) and immediately after (0.06–0.10) it. We then constructed the average of normalized eclipse profiles. We show both the average and the individual profiles in the right half of Figure 5. We confirm that the reduction in count rate is seen every time the eclipse phase is observed. At the same time, there are variations in the light curves from cycle to cycle. This is most apparent in the egress for cycle 4, for which two interpretations are possible. Either the egress was delayed by ∼0.008 cycle or the total emission was lower by 30–40% during the egress. Although there is less disagreement on the ingress side, the profile there may be similarly affected by cycle to cycle variability.

To summarize, we observe a significant decline in the X-ray count rates during the phase of the optical eclipse (Figure 4). This feature is present every cycle, the fractional decrease is independent of the photon energy, but there are variations in the detailed profile from cycle to cycle (Figure 5). We conclude that we have discovered a partial eclipse of the X-ray emitting region by the secondary in V893 Sco.

4. Discussion

4.1. Intrinsic Absorber and Abundances

First, we comment on two issues that do not affect our understanding of V893 Sco significantly. Rather, these are issues that should be kept in mind in studies of other CVs.

One is the presence of intrinsic absorber that required a partial-covering absorption model to fit (Table 2). Ramsay et al. (2008) have studied the spectra of 3 systems that they consider to be IP candidates, and cite the presence of a complex absorber in all 3 systems as a supporting evidence for their IP classification. Of the three, EI UMa, has recently been confirmed as an IP (see also Reimer et al. 2008) and its partial covering absorber has N_H= 4.5 $\times 10^{22}$ cm^{-2} (covering fraction of 67%), higher than $\sim 1.3 \times 10^{22}$ cm^{-2} (73%) that we derive for V893 Sco. In turn, the partial covering absorber in V893 Sco has a higher column than those in LS Peg and V426 Oph that Ramsay et al. (2008) derived. By their logic, V893 Sco must then be considered an IP candidate. Yet, as previously mentioned (§1), existing optical data argue against an IP classification of V893 Sco; we will also argue below (§4.3) that the partial X-ray eclipse makes an IP interpretation problematic. As van Teeseling et al. (1996) showed, a strong intrinsic absorption is a general phenomenon among high inclination non-magnetic CVs . This absorber is likely located in the inner disk near the boundary layer; such an absorber, comparable in size to the X-ray emission region, would naturally result in partial-covering absorption. Our result on V893 Sco strongly suggests that a partial covering absorber at the $\sim 10^{22}$ cm^{-2} level in a high inclination CV does not necessarily imply the system to be an IP. Although a higher N_H and/or a presence of a complex absorber in a low inclination system may yet turn out to be a strong evidence for an IP, a quantitative study is required to establish this as a secure method of identifying IPs.

The second point is that the abundances one derives is dependent on the spectral model one uses (Table 2). In the case of V893 Sco, a single temperature `mekal` fit requires a lower abundance than a cooling flow (`mkcflow`) fit. This is because a temperature near the peak of He-like Fe Kα emissivity is found in the `mekal` case, while the cooling flow fits find a range of temperatures including those at which the Fe Kα line emissivity is low. To reproduce the observed line strength, therefore, a lower Fe abundance is required with the `mekal` fit than with the `mkcflow` fit. Similarly, single absorber fits require higher temperatures to match the observed, hard, continuum slope, lowering the line emissivity. Thus single absorber fits result in higher abundance than the complex absorber fits. We believe this to be a general concern in the analysis of any CCD-resolution X-ray spectra of CVs in which the Fe Kα complex is the only discrete spectra feature detected. For this reason, we do not comment on the abundances in V893 Sco in this work. It is far better to use data that show multiple lines features, e.g., *XMM-Newton* RGS data (Pandel et al. 2005).

4.2. X-ray Luminosity and Temperature of V893 Sco

We infer that the bolometric X-ray luminosity of V893 Sco to be 1.0–1.4×10^{32} ergs s^{-1} at the time of the *Suzaku* observations. The possibility that it may have higher X-ray luminosity at other epochs has been suggested by the RASS and XSS count rates, although caution is warranted since the former has a limited bandpass and the latter is non-imaging. In any case, V893 Sco appears to be among the most X-ray luminous dwarf nova.

What makes V893 Sco X-ray bright? This is an important question that has a bearing on the physics of accretion disk at low mass transfer rate. However, we believe it is best addressed in the context of a comparative study using data on a number of systems with different X-ray luminosity levels. Similarly, an important motivation of the XSS was to reassess the contribution of low luminosity objects to the Galactic ridge X-ray emission. This, too, should be addressed in a collective study.

In our single-temperature `mekal` fits, we found plasma temperatures of 9.4 and 6.7 keV, depending on the absorption model used. This is within the range of temperature found by Baskill et al. (2005) (roughly 3–10 keV) for dwarf novae observed with *ASCA* using the same procedure. In contrast, fits to <10 keV spectra of IPs tend to find very high, often unconstrained temperatures. For example, Baskill et al. (2005) found kT>77 keV for EI UMa, which was included in their compilation because its magnetic nature was unknown at the time. That is, V893 Sco appears similar to other dwarf novae in terms of the Temperature, and would be atypical for an IP.

4.3. The Partial X-ray Eclipse

The detection of a partial eclipse in a non-magnetic CV is unprecedented. All previous observations of deeply eclipsing, quiescent dwarf novae showed flat-bottomed X-ray eclipses that are consistent with being total, perhaps except for a weak residual contribution from the corona of the secondary (Wood et al. 1995; van Teeseling 1997; Mukai et al. 1997; Pratt et al. 1999; Ramsay et al. 2001; Wheatley & West 2003). The transitions into and out of eclipses have been used to constrain the total size of the X-ray emission region to be not much larger than the white dwarf.

X-ray emission from regions other than the vicinity of the white dwarf and from the corona of the secondary have been considered in the literature. One speculated source is the bright spot region. However, this possibility was comprehensively refuted by Pringle (1977); in particular, the highest shock temperature possible for the bright spot is of order kT∼1 keV, and therefore this can be discarded for V893 Sco. The other is a known source of soft

X-rays in high accretion rate systems. For example, in the *XMM-Newton* observations of the eclipsing nova-like system, UX UMa, Pratt et al. (2004) have found two components of X-ray emission. One is highly absorbed and undergoes a total eclipse, and therefore originates from a compact region around the white dwarf. The other is a soft, unabsorbed componet that does not show total or partial eclipse, and is therefore from an highly extended region. This component has the wrong spectral shape and its origin is far too extended, and therefore cannot be the explanation for the partially eclipsed component in V893 Sco.

We believe that a grazing geometry in which the entire photosphere of the white dwarf is never completely eclipsed can explain both the optical and the X-ray eclipse profiles. To see that such a geometry is not too contrived, let us take a plausible set of system parameters and estimate the probability of a partial eclipse of the white dwarf. Given the 1.82 hr orbital period, an assumed mass ratio of 0.25, an empirical mass-radius relationship of the secondary (Patterson 1984), and a white dwarf mass-radius relationship (Pringle & Webbink 1975), we estimate the secondary radius R_2 of 1.28×10^{10} cm, the primary radius R_1 of 8.86×10^{8} cm, and a binary separation a of 4.73×10^{10} cm (see Table 5). With these representative numbers, and approximating the Roche-lobe filling secondary as a sphere, the bottom of the white dwarf is just eclipsed at an inclination angle i of 73.88°; the top at i=75.88°, compared to the range of 75.88°–90° for a total eclipse. This implies that the white dwarf photosphere is partially eclipsed in over 10% of the eclipsing CVs with such system parameters. The key factor is the ratio of the white dwarf diameter to the radius of the secondary, which is $\sim$1/7 in this case, and this should be the approximate ratio of systems with partial and total eclipses of the white dwarf photosphere.

Total eclipse of the white dwarf must result in a double eclipse (§1) and vice versa.. According to RKcat, there are 13 dwarf novae below the period gap in which double eclipses are known (Table 1). The true number of double eclipse dwarf novae is likely to be higher, because there may be systems in this table that are too faint and/or too recently discovered to have high time resolution, high signal-to-noise photometry necessary for a double eclipse to have been discovered. We therefore expect $\sim$2 systems in this table to have a partial eclipse of the white dwarf photosphere. As the white dwarf is a major source of visible light (along with the bright spot) in a quiescent dwarf nova below the period gap, such a system should have a relatively shallow eclipse that is not flat-bottomed, just as is observed in V893 Sco.

We now consider the X-ray eclipse in such a system assuming three different geometry of the X-ray emission region. Magnetic pole region(s) as appropriate for IPs, a spherical corona that covers the entire white dwarf photosphere, and an equatorial boundary layer. We sketch a possible geometry for the boundary layer case in Figure 6.

The accretion in IPs, by definition, occurs onto an area smaller than the entire surface of the white dwarf. For the IP, XY Ari, Hellier (1997) used the sharpness and the changing timing of eclipse egresses to infer small (<0.002 of the total surface area) spots that move on the projected face of the white dwarf as a function of the spin phase. It's extremely unlikely that such a small spot be partially eclipsed by the secondary. Thus, if V893 Sco is an IP, it must have much larger spots than Hellier (1997) found in XY Ari. If two larger spots are located near the rotational poles, a flat-bottomed partial eclipse is a likely result, as we do indeed observe in EX Hya (where the lower pole is always eclipsed and the upper pole is never eclipsed; see Rosen et al. 1991). If the lower pole is never observable, then the upper pole must be very close to the rotational pole. To produce a deep partial eclipse of X-rays from such an upper pole, most of the white dwarf surface must be eclipsed, in which case we expect a deeper eclipse in the optical. If both poles are on or near the equator, we should observe a significant jitter in the eclipse timing (corresponding to a significant fraction of the width of the optical eclipse) and/or two distinct sets of ingress/egress during a single X-ray eclipse. The latter has not been observed, while the possible phase jitter is 0.008 (Figure 5), less than 30% of the total eclipse duration (0.03; see Table 4). Thus, even with a much larger spot size than that seen in XY Ari, a rather contrived set of circumstances are required to explain our X-ray observations. We therefore argue that the X-ray light curves point to V893 Sco being a genuine, non-magnetic dwarf nova, just as optical observations indicated.

Next, we consider a spherical corona surrounding the white dwarf. This simple scenario has the advantage that, if the white dwarf photosphere is partially eclipsed, so must be the corona. Because such a corona is bigger then the white dwarf in every direction, the eclipse must last longer: this does not appear to be the case, although such an interpretation may still be viable once we allow for cycle-to-cycle variability. The geometry also dictates that the depth of the eclipses be similar between the X-rays and the photospheric emission. In contrast, the X-ray eclipse appears deeper than the optical eclipse. Another consequences of this geometry is that the eclipse should be U-shaped, from the limb brightening of an optically thin emission plus the fact that the body of the white dwarf blocks the emission from the far side. This, again, does not appear to be the case. We therefore argue that this scenario is also not likely, although further observations are required to reach a definite conclusion.

Finally, we consider the boundary layer picture. We must first consider whether a partial eclipse of an equatorial boundary layer is likely. This turns out not to be a severe problem. The reason for this is that, due to the inclination of $\sim 75^\circ$, the projected equator of the white dwarf is significantly curved, spanning $\sim$1/8 of the white dwarf diameter. Thus, even a smallest possible boundary layer of a negligible height and a negligible extent in latitude will suffer a partial eclipse in $\sim$1/8 of the partial eclipsing dwarf nova. The probability can

only rise with any spatial extent of the boundary layer.

In Figure 7, we reproduce the observed optical and X-ray eclipse profiles. We have changed the scaling of optical data from magnitude scale to linear flux scale, and we use the normalized then averaged X-ray light curve (Figure 5).

The model light curves and the schematic diagrams (Figure 6) were produced using the same set of computer codes to check for their accuracy. We also used the same exact set of parameters in both, including the system parameters noted above. We further used an inclination of 74.2°, which results in a less than half the white dwarf disk getting eclipsed. For the optical light curves, we only show the eclipse of the white dwarf, assumed to have no limb darkening here. In our geometry, the bright spot (whose location and spatial extent is admittedly uncertain) should be fully eclipsed during most, if not all, of the white dwarf eclipse, and other sources of light is expected to be negligible. As to limb darkening, we have also simulated a case with an extreme limb darkening (u=1 following, and using the notation of, Wood & Horne 1990), but this does not make a large enough difference to matter here. The vertical dashed lines in Figure 7 are the ingress and egress timings we measured and used to adjust the orbital ephemeris (§3.2 and Table 4).

We provide two models of the X-ray light curve. In one (green), we assumed a spherical corona with a height of $0.2R_1$. For the other (red), we assumed a boundary layer that extends $\pm5°$ from the equator in latitude, and an X-ray emission region height of $0.2R_1$. Both our optical and X-ray (boundary layer) models reproduce the gross features of the observed light curves, although there are disagreements in detail. Note that, although we have adjusted several parameters to achieve this match, this is not a fit. Our intention here is to demonstrate the feasibility of, and the promise of, this class of models.

To proceed to the next level of actually fitting the optical and X-ray light curves, several things must happen. First, the system parameters must be constrained from UV, optical, and IR observations to narrow down the parameter space. UV spectroscopy in particular is useful in constraining the white dwarf parameters (Godon et al. 2008), and has the potential to confirm or refute the partial eclipse of its photosphere. Any constraints on the white dwarf and secondary masses and sizes and on inclination will help in future modeling of the eclipse light curves.

Second, the quality of the X-ray light curve must improve. The statistical quality is one issue, but we also need to observe an increased number of X-ray eclipses to average out cycle-to-cycle variations, and to search for signatures of moving spots expected in IPs. Observations from high Earth orbit will help in allowing a better modeling of the longer-term (minutes to hours) variability and to separate that from the eclipse profile.

5. Conclusions

We performed *Suzaku* observations of the eclipsing dwarf nova, V893 Sco. We confirm that it is an X-ray luminous dwarf nova, and moreover, report the discovery of a partial X-ray eclipse.

In the past, both optical and X-ray observers have concentrated on systems that exhibit a total eclipse of the white dwarf. They provide a strong constraint on the height of the X-ray emission region above the white dwarf. However, as our initial modeling effort shows, partially eclipsing systems may allow the shape of the X-ray emission region to be determined, because the eclipse shapes are sensitive to the extent of the region in latitude. The *Suzaku* X-ray light curve already disfavors a spherical corona. Future X-ray observations, together with improved estimates of system parameters from other wavelengths, have the potential to confirm the boundary layer picture of X-ray emission in quiescent dwarf novae, and furthermore to constrain the latitudinal extent of such a boundary layer.

This research has made use of data obtained from the *Suzaku* satellite, a collaborative mission between the space agencies of Japan (JAXA) and the USA (NASA).

REFERENCES

Baskill, D. S., Wheatley, P. J. & Osborne, J. P. 2005, MNRAS, 375, 626

Bruch, A., Steiner, J. E. & Gneiding, C.D. 2000, PASP, 112, 237

Cropper, M., Wu, K., Ramsay, G. & Kocabiyik, A. 1999, MNRAS,306, 684

Dickey, J.M. & Lockman, F.J. 1990, ARA&A, 28, 215

Done, C. & Osborne, J.P. 1999, MNRAS, 288, 649

Godon, P., SIon, E. M., Barrett, P. E., Hubeny, I., Linnell, A. P. & Szkody, P., ApJ, in press (astro-ph/0802.2022)

Hellier, C. 1997, MNRAS, 291, 71

Kato, T., Haseda, K., Takmizawa, K., Kazarovets, E. V. & Samus, N. N. 1998, IBVS, 4585

Kato, T., Matsumoto, K. & Uemura, M. 2002, IBVS, 5652

Lasota, J.-P. 2001, New Astronomy Reviews, 45, 449

Livio, M. & Pringle, J.E. 1992, MNRAS, 259, 23P

Mason, E., Skidmore, W., Howell, S.B. & Mennickent, R.E. 2001, ApJ, 563, 351

Matsumoto, K., Mennickent, R. E. & Kato, T. 2000, A&A, 363, 1029

Meyer, F. & Meyer-Hofmeister, E. 1994, A&A, 288, 175

Mhlahlo, N., Buckley, D.A.H., Dhillon, V.S., Potter, S.B., Warner, B. & Woudt, P.A. 2007, MNRAS, 380, 353

Mitsuda, K. et al., 2007, PASJ, 59, S1

Mukai, K., Wood, J. H., Naylor, T., Schlegel, E. M. & Swank, J. H. 1997, ApJ, 475, 812

Mukai, K., Kinkhabwala, A., Peterson, J. R., Kahn, S. M. & Paerels, F. 2003, ApJ, 586, L77

O'Donoghue, D. 1995, Balt. Astron. 4, 519

Pandel, D., Córdova, F. A., Mason, K. O. & Priedhorsky, W. C. 2005, ApJ, 626, 396

Patterson, J. 1984, ApJS, 54, 443

Patterson, J. & Raymond, J.C. 1985, ApJ, 292, 535

Patterson, J., 1994, PASP, 106, 209

Pratt, G. W., Hassall, B. J. M., Naylor, T. & Wood, J. H., 1999, MNRAS, 307, 413

Pratt, G. W., Mukai, K., Hassall, B. J. M., Naylor, T. & Wood, J. H., 2004, MNRAS, 348, 49

Pretorius, M.L., Warner, B. & Woudt, P.A. 2006, MNRAS, 368, 361

Pringle, J. E. & Webbink, R. F. 1975, MNRAS, 172, 493

Pringle, J. E. 1977, MNRAS, 178, 195

Ramsay, G., Poole, T., Mason, K., Córdova, F., Priedhorsky, P., Breeveld, A., Much, R., Osborne, J., Pandel, D., Potter, S., West, J. & Wheatley, P. 2001, A&A, 365, 288

Ramsay, G., Wheatley, P.J., Norton, A.J., Hakala, P. & Baskill, D. 2008, MNRAS, in press (astro-ph/0804.1223)

Reimer, T.W., Welsh, W.F., Mukai, K. & Ringwald, F.A. 2008, ApJ, 678, 384

Revnivtsev, M., Sazonov, S., Jahoda, K. & Gilfanov, M. A&A, 418, 927

Ritter, H. & Kolb, U. 2003, A&A, 404, 301

Rosen, S. R., Mason, K. O., Mukai, K. & Williams, O. R. 1991, MNRAS, 249, 417

Schechter, P.L., Mateo, M. & Saha, A. 1993, PASP, 105, 1342

Thorstensen, J. 1999, IBVS, 4749

Thorstensen, J. 2003, AJ, 126, 3017

van Teeseling, A., Beuermann, K. & Verbunt, F. 1996, A&A, 315, 467

van Teeseling A. 1997, A&A, 319, L25

Warner 1995, *Cataclysmic Variables* (Cambridge: Cambridge Univ. Press)

Warner, B., Woudt, P.A. & Pretorius, M.L. 2003, MNRAS, 344, 1193.

Wheatley, P. J. & West, R. G., MNRAS, 345, 1009

Wood, J. H. & Horne, K. 1990, MNRAS, 242, 606

Wood, J. H., Naylor, T., Hassall, B. J. M. & Ramseyer, T. 1995, MNRAS, 273, 772

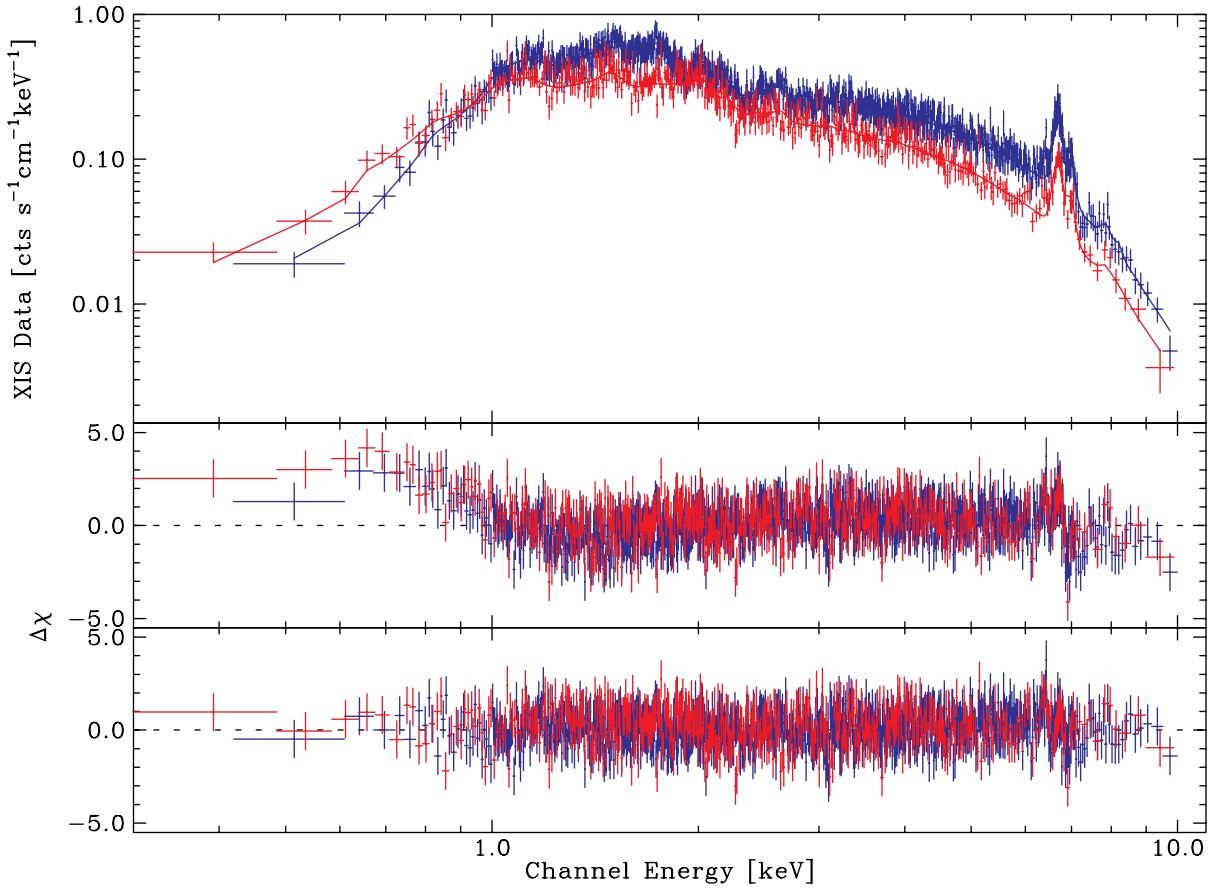

Fig. 1.— The *Suzaku* XIS spectra (blue: sum of three units with FI CCDs; red: XIS1 data, containing the BI CCD) of V893 Sco fitted with the cooling flow (`mkcflow`) model. The data are shown in the top panel. The middle panel shows the residuals when only a simple absorber is used. The bottom panel shows the residuals with a simple and a partial covering absorber. The solid line on the top panel shows the latter model.

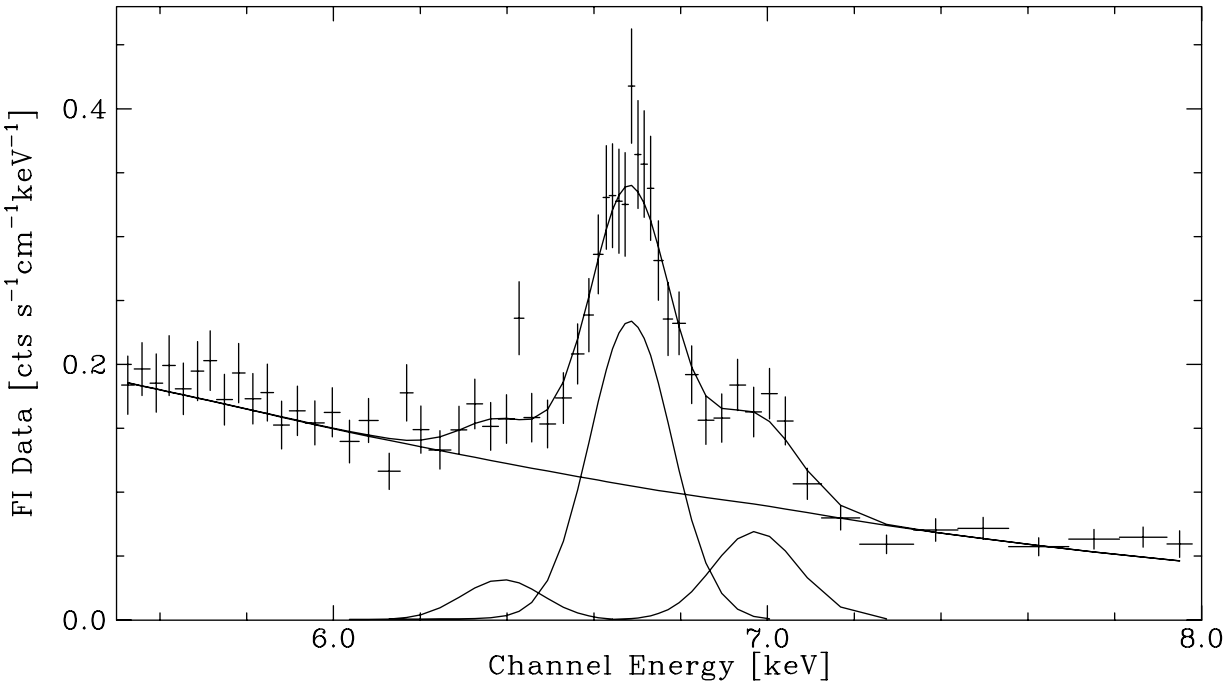

Fig. 2.— The FI CCD spectrum of V893 Sco in the Fe Kα region. The He-like line at 6.7 keV is the dominant component. The 6.4 keV and 6.97 keV components are also detected but are weaker.

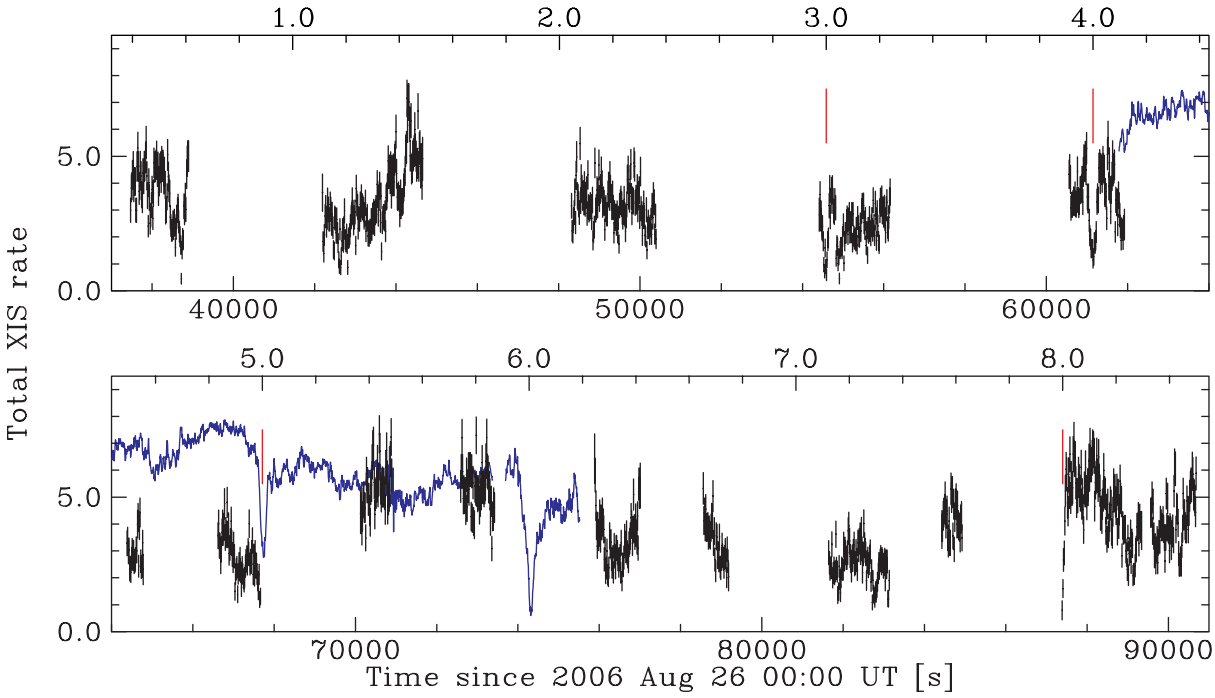

Fig. 3.— The X-ray light curve (black) of V893 Sco in 16 s bins plotted against time (bottom axis) and, equivalently, relative cycle counts (top axis). The Aug 26 SAAO photometry is shown in blue. Red tick marks shows the two full and two partial coverage of the eclipse phase by the *Suzaku* XIS.

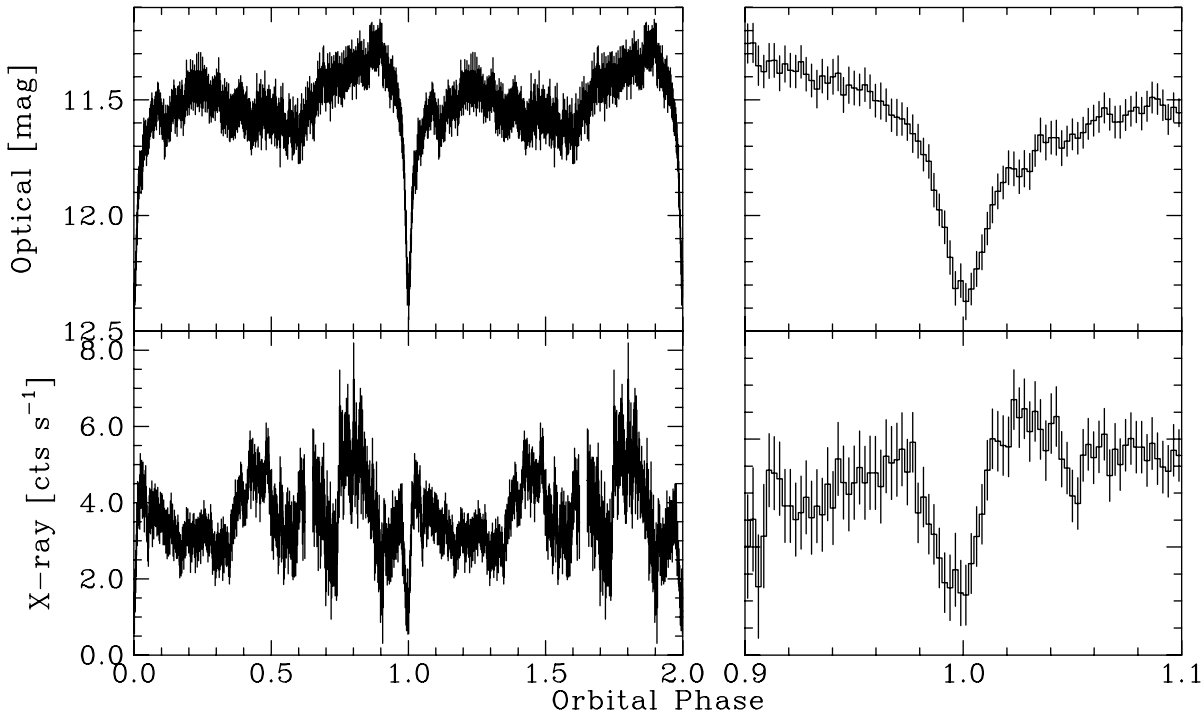

Fig. 4.— Folded light curves of V893 Sco from our SAAO (top) and *Suzaku* (bottom) observations. Left panels show the two complete cycles, while the right panels focus in on the eclipse phase. Note that the optical light curves are plotted in magnitude scale; see Figure 7 for a linear version.

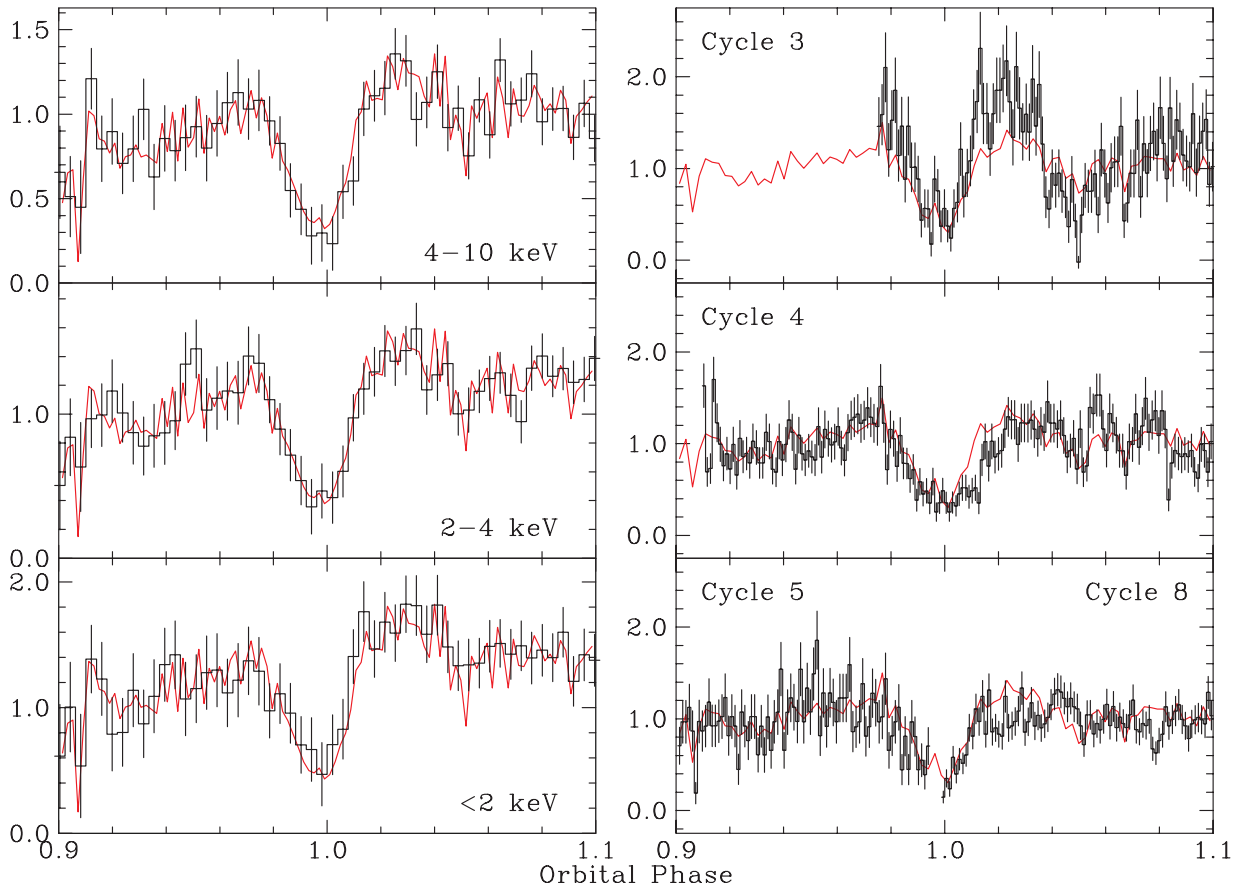

Fig. 5.— (Left) The X-ray eclipses in three energy ranges. In each panel, the histograms show the data in the energy range shown, while the solid line is the total (0.3–10 keV) light curve. All curves are scaled such that the top of the panel is 1.2 times the largest bin. (Right) The individual cycles of the X-ray eclipse. In each panel, the histograms show an individual eclipse (the ingress during cycle 5 and the egress during cycle 8 for the bottom panel), while the solid line is for the average curve. All curves are scaled to the out-of-eclipse value (see text for details).

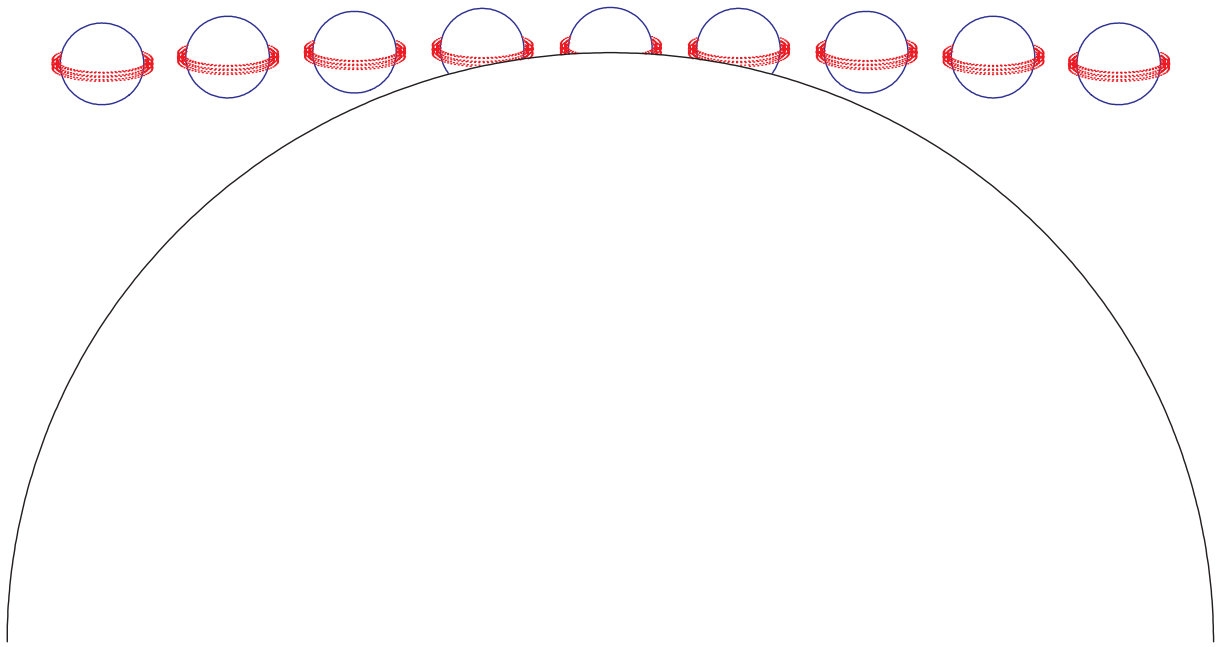

Fig. 6.— A schematic diagram of the possible geometry of the grazing eclipse in V893 Sco.

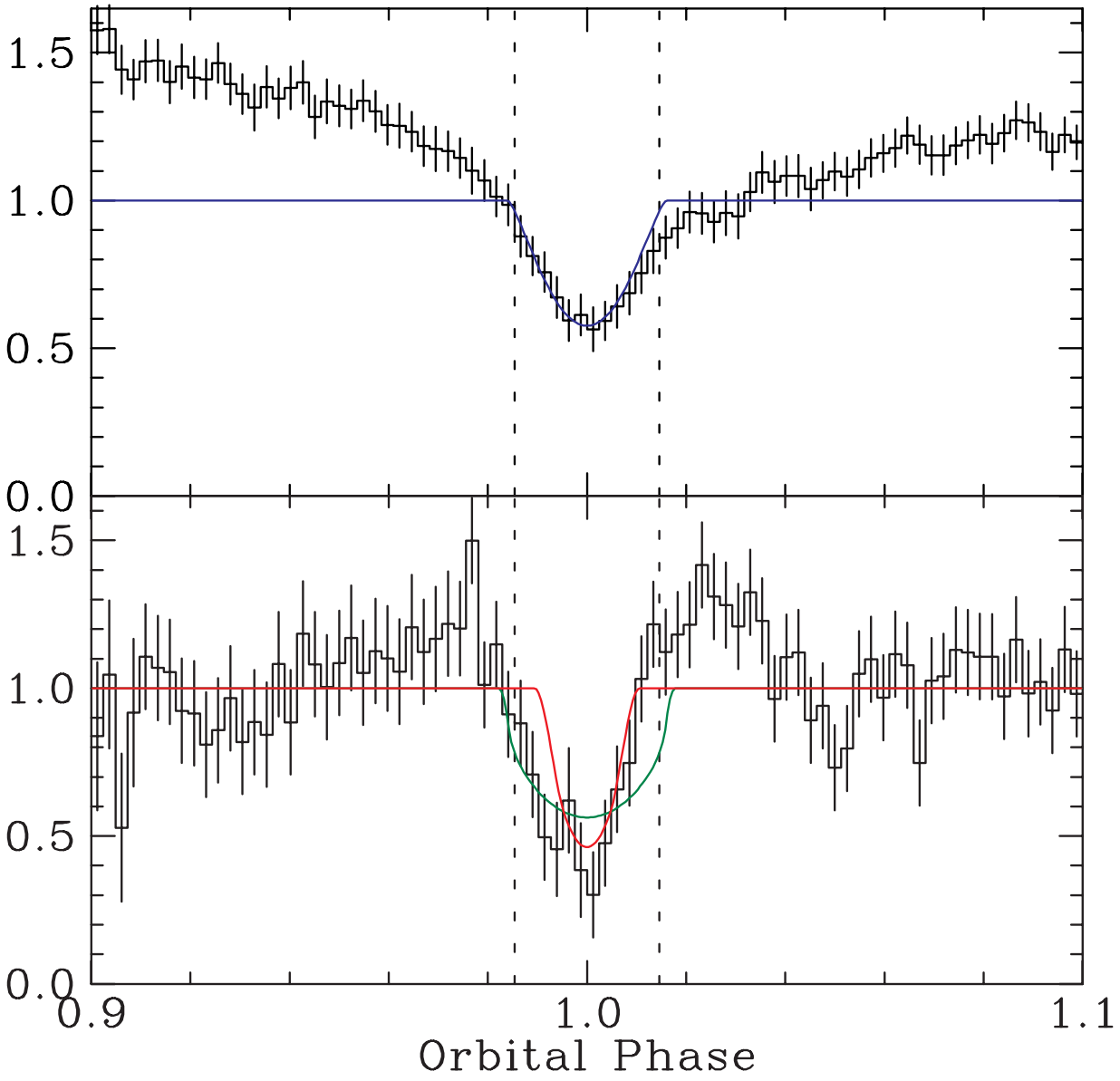

Fig. 7.— Optical and X-ray eclipse light curves plotted with representative models (see text).

Table 1. Eclipsing Dwarf Novae and Candidates[a] Below the Period Gap.

Name	Max. magnitude[b]	Mid-Eclipse	Period (d)	Double?[c]
WZ Sge	15.0	15.6	0.056688	
V2051 Oph	15.0	17.5	0.062428	Y
Z Cha	15.5	17.3	0.074499	Y
V893 Sco	15.5		0.075962	
V455 And	16.1	16.5	0.056309	
HT Cas	16.4	18.4	0.073647	Y
OY Car	16.7	18.0	0.063121	Y
IR Com	16.9	19.0	0.087039	
SDSS J150240.98+333423.9	17.0	19.6	0.0585	
CC Scl	17.3	17.6	0.0587	
IY UMa	17.3	19.3	0.073909	Y
V4140 Sgr	17.5	19.0	0.061430	
OU Vir	17.5	19.3	0.07273	Y
V713 Cep	18.0	>21.0	0.08542	
CTCV J1300-3052	18.0	22.1	0.08898:	Y
SDSS J150722.33+523039.8	18.1	19.6	0.046258	Y
SDSS J143317.78+101123.3	18.2g	21.0g	0.0543	Y
DV UMa	18.3	20.8	0.085853	Y
Hα 0242−2802	18.4	21.7	0.0746	Y
XZ Eri	18.8	20.6	0.061159	Y
SDSS J103533.03+055158.4	18.8g		0.057007	Y
SDSS J155656.92+352336.6	18.9	20.4	0.0892	
CTCV J2354−4700	18.9	20.5	0.06554	
SDSS J122740.83+513925.0	19.1		0.06296	
SDSS J090403.48+035501.2	19.2g		0.0597	
SDSS J090103.93+480911.1	19.3		0.0779	
SDSS J155531.99−001055.0	19.3	21.	0.07885	
SDSS J150137.22+550123.4	19.4	21.0	0.0542	

[a]These objects either have a "dwarf nova" classification or an unknown sub-type in RKcat 7.9

[b]Out-of-eclipse magnitude in quiescence

[c]Systems in which eclipse of the white dwarf and of the bright spot has been established

Table 2. Spectral Parameters of V893 Sco.

Model	χ^2_ν	N_H (10^{21} cm^{-2})	$N_{H,2}$ (10^{22} cm^{-2})	CF[a]	kT/kT$_{max}$ (keV)	Abund.	L_x[b] (ergs s^{-1})
mekal	1.006	$5.14^{+0.18}_{-0.16}$			$9.43^{+0.42}_{-0.39}$	$0.94^{+0.06}_{-0.07}$	1.08×10^{32}
mekal	0.774	$2.86^{+0.25}_{-0.28}$	$1.87^{+0.27}_{-0.23}$	$0.52^{+0.03}_{-0.04}$	$6.73^{+0.34}_{-0.31}$	$0.66^{+0.06}_{-0.05}$	1.14×10^{32}
mkcflow	0.999	$6.45^{+0.10}_{-0.29}$			$32.9^{+2.7}_{-1.9}$	$1.17^{+0.10}_{-0.09}$	1.43×10^{32}
mkcflow	0.766	$2.51^{+0.53}_{-0.48}$	$1.28^{+0.14}_{-0.05}$	$0.73^{+0.01}_{-0.05}$	$16.6^{+1.2}_{-1.3}$	$0.87^{+0.08}_{-0.07}$	1.38×10^{32}

[a]Covering Fraction of the partial covering absorber

[b]Extrapolated X-ray luminosity in the 0.01–100 keV range, which is a good approximation of the bolometric X-ray luminosity, assuming a distance of 155 pc.

Table 3. Fe Kα Lines V893 Sco.

Energy (keV)	σ (eV)	Eq.W (eV)[a]
6.40±0.04	<70	40±15
6.69±0.01	<350	400±30
6.99±0.02	<40	100±20

[a]Errors on the equivalent widths have been estimated assuming continuum flux is accurately known

Table 4. Optical Eclipse Timings of V893 Sco.

Eclipse	Transition	HJD	Decline (mag)	Bruch et al. Phase
Aug 25-1	Ingress	2453973.29557	0.63	0.81096
Aug 25-1	Egress	2453973.29786	0.51	0.84113
Aug 25-2	Ingress	2453973.37131	0.54	0.80805
Aug 25-2	Egress	2453973.37367	0.41	0.83913
Aug 26-1	Ingress	2453974.28288	0.55	0.80841
Aug 26-1	Egress	2453974.28531	0.64	0.84041
Aug 26-2	Ingress	2453974.35892	0.56	0.80946
Aug 26-2	Egress	2453974.36122	0.45	0.83963
Aug 27-1	Ingress	2453975.27046	0.57	0.80936
Aug 27-1	Egress	2453975.27243	0.48	0.83528
Aug 27-2	Ingress	2453975.34644	0.40	0.80965
Aug 27-2	Egress	2453975.34839	0.48	0.83525
Average	Ingress		0.56±0.02	0.8093±0.0005
Average	Egress		0.47±0.04	0.8385±0.0011

Table 5. Assumed System Parameters

Mass Ratio	Inclination	Separation	M_1	R_1	M_2	R_2
0.25	74.2	4.73×10^{10} cm	0.58 $M_\odot$	8.86×10^{8} cm	0.15 $M_\odot$	1.28×10^{10} cm